

# Extensive networks would eliminate the demand for pricing formulas

Jaegi Jeon<sup>a</sup>, Kyunghyun Park<sup>a</sup>, Jeonggyu Huh<sup>b,\*</sup>

<sup>a</sup>Department of Mathematical Sciences, Seoul National University, Seoul 08826, Korea

<sup>b</sup>Department of Statistics, Chonnam National University, Gwangju 61186, Korea

---

## Abstract

In this study, we generate a large number of implied volatilities for the Stochastic Alpha Beta Rho (SABR) model using a graphics processing unit (GPU) based simulation and enable an extensive neural network to learn them. This model does not have any exact pricing formulas for vanilla options, and neural networks have an outstanding ability to approximate various functions. Surprisingly, the network reduces the simulation noises by itself, thereby achieving as much accuracy as the Monte-Carlo simulation. Extremely high accuracy cannot be attained via existing approximate formulas. Moreover, the network is as efficient as the approaches based on the formulas. When evaluating based on high accuracy and efficiency, extensive networks can eliminate the necessity of the pricing formulas for the SABR model. Another significant contribution is that a novel method is proposed to examine the errors based on nonlinear regression. This approach is easily extendable to other pricing models for which it is hard to induce analytic formulas.

*Keywords:* efficient pricing; deep learning; SABR model; nonlinear regression; GPU-based simulation; neural network

---

## 1. Introduction

Neural networks are often employed for regression because they have an outstanding ability to approximate a wide range of functions (refer to Cybenko [1] and Hornik et al. [2] for the celebrated universal approximation theorem). Only a decade ago, simple models, such as linear models, were preferred over neural networks. Most researchers used to believe that too many parameters led to notorious overfitting, which has resulted in an artificial intelligence winter in the past. However, as numerous techniques have been invented to prevent such an occurrence, most researchers like to utilize such networks in their research. To review the literature concerning the application of networks in finance, refer to Ruf and Wang [3] for network-based option pricing and Henrique et al. [4] for market predictions.

Since the work of Hutchinson et al. [5], many researchers have been studying artificial neural networks to predict the option prices  $c$  (or the implied volatilities  $\sigma^I$ ) for particular parametric models, such as the Black-Scholes model [6], the Heston model [7], and the SABR model [8]. We selected six related studies [9, 10, 11, 12, 13, 14] and summarized their approaches in Tables 1 and 2. Interestingly, we can observe similar propensities in the studies. They mainly focus on the models that can provide efficient pricing formulas for vanilla options such as the Black-Scholes model and the Heston model. For instance, the Heston model gives a closed-form characteristic function, enabling cost-effective option pricing through a Fourier transform [15]. Note that all works other than McGhee [12] are either associated with the Black-Scholes model or the Heston model. This correlation may exist because training samples are generated exhaustively to eliminate the necessity of numerical algorithms. We, however, think that their contributions are a little marginal from a practical perspective as even without the networks, the option prices can already be efficiently obtained.

---

\*corresponding author.

E-mail address: huhjeonggyu@jnu.ac.kr

	Culkin (2017)	Brostrom (2018)	Ferguson (2018)	McGhee (2018)
base model	Black-Scholes	Black-Scholes	Black-Scholes	SABR ( $\beta = 1$ )
options type	vanilla	vanilla	basket	vanilla
pricing method	closed formula	closed formula	MC simulation	finite difference method
network inputs	$f_0/K, T, r, q, \bar{\alpha}$	$f_0/K, T, r, \bar{\alpha}$	$f_{0i}/K, T, \bar{\alpha}_i, \rho_{ij}$ ( $1 \leq i, j \leq 6$ )	$f_0/K, T, \alpha_0, \nu, \rho$
network outputs	$c/K$	$c/K$	$c/K$	$\sigma^I$
# of training samples (precision)	240k (exact)	800k (exact)	500M (10k paths)	2.5M ( $\{n_t, n_f, n_\alpha\} = \{400, 200, 100\}$ )
# of test samples (precision)	60k (exact)	200k (exact)	5k (100M paths) [?]	500k ( $\{n_t, n_f, n_\alpha\} = \{400, 200, 100\}$ )
# of epochs	10	50	95 [?]	N/A
batch size	64	200	50k	N/A
# of hidden layers	4	2	6	1
# of nodes per layer	100	256	1,400	1,000
activation functions	ReLU, ELU, etc.	ReLU	ReLU	softplus, ReLU
optimizer	SGD	ADAM	ADAM	ADAM
architecture tuning	none	# of layers, # of nodes	# of nodes	# of nodes
test loss MSFE	1.25E-4	7.27E-8	5E-5 [?]	N/A
test loss MSPE	same as above	same as above	N/A	N/A

Table 1: This table outlines various methods to train neural networks using option prices  $c$  (or implied volatilities  $\sigma^I$ ). If there are several results in a work, only the best is written here. The base models are expressed as follows:  $df_t = (r - q)ftdt + \bar{\alpha}fdW_t$  (Black-Scholes),  $df_t = (r - q)fdt + \sqrt{y_t}f_t dW_t$ ,  $dy_t = \kappa(\bar{y} - y_t) + \nu\sqrt{y_t}dZ_t$  (Heston),  $df_t = \alpha_t f_t^\beta dW_t$ ,  $d\alpha_t = \nu\alpha_t dZ_t$  (Stochastic Alpha Beta Rho [SABR]), where  $dW_t/dZ_t = \rho dt$ .  $K$  and  $T$  are the strike and maturity of the vanilla option, respectively. The LR, SGD, MSFE, and MSPE stand for the learning rate, the stochastic gradient descent, the mean squared fitting error, and the mean squared prediction error, respectively (refer to Section 2 for the MSFE and MSPE). Finally, we used prefixes for the international system of units:  $1k = 1000$  and  $1M = 1000k$ . The mark [?] indicates that the value is inferred using the context or the figures in the work.

	Liu (2019)		Hirsa (2019)		our method (2020)	
base model	Black-Scholes	Heston	Black-Scholes	Heston	SABR ( $\beta = 1$ )	
options type	vanilla	vanilla	vanilla	vanilla	vanilla	vanilla
pricing method	closed formula	Fourier-cosine series	closed formula	fast Fourier transform	MC simulation	
network inputs	$f_0/K, T, r, \bar{\alpha}$	$f_0/K, T, r, y_0, \kappa, \bar{y}, \nu, \rho$	$f_0/K, T, r, q, \bar{\alpha}$	$f_0/K, T, r, q, y_0, \kappa, \bar{y}, \nu, \rho$	$K/f_0, T, \alpha_0, \nu, \rho$	
network outputs	$c/K, \sigma^I$	$c, \sigma^I$	$c/K$	$c/K$	$\sigma^I$	
# of training samples (precision)	900k (exact)	900k (800k+100k) (almost exact)	240k (exact)	240k (almost exact)	520M (480M+40M) (500k paths)	
# of test samples (precision)	100k (exact)	100k (almost exact)	60k (exact)	60k (almost exact)	140M (40M+100M) (500k, 12.5M paths)	
# of epochs		3000		N/A	early stopping	
batch size		1024		N/A	100	
# of hidden layers		4		4	2	
# of nodes per layer		400		120	7,000	
activation functions		ReLU		ReLU, ELU, etc.	ReLU	
optimizer		LR decaying ADAM		ADAM	LR decaying ADAM	
architecture tuning		# of nodes		# of layers, # of nodes	# of layers, # of nodes	
test loss	MSFE	8.21E-9 ( $c/K$ )	1.65E-8 ( $c$ )	1.8E-5 [?]	2.5E-5 [?]	5.5E-6
	MSPE	1.55E-8 ( $\sigma^I$ )	5.07E-7 ( $\sigma^I$ )	same as above	same as above	2.0E-7

Table 2: This table summarizes methods to train neural networks using option prices  $c$  (or implied volatilities  $\sigma^I$ ). If there are several results in a work, only the best is written here. The base models are expressed as follows:  $df_t = (r - q) f_t dt + \bar{\alpha} f_t dW_t$  (Black-Scholes),  $df_t = (r - q) f_t dt + \sqrt{y_t} f_t dW_t$ ,  $dy_t = \kappa (\bar{y} - y_t) + \nu \sqrt{y_t} dZ_t$  (Heston),  $df_t = \alpha_t f_t^\beta dW_t$ ,  $d\alpha_t = \nu \alpha_t dZ_t$  (SABR), where  $dW_t dZ_t = \rho dt$ . In particular,  $K$  and  $T$  are the strike and maturity of the vanilla option, respectively. The LR, SGD, MSFE, and MSPE stand for a learning rate, the stochastic gradient descent, the mean squared prediction error, and the mean squared fitting error, respectively (refer to Section 2 for the MSFE and MSPE). Finally, we used prefixes for the international system of units: 1k = 1000 and 1M = 1000k. The mark [?] signifies that the value is deduced using the context or the figures in the work.

Notably, McGhee [12] aimed to allow a neural network to learn the vanilla option prices for the SABR model. The model does not offer exact and efficient solutions for a true option value  $c_{true}$ . Thus, a finite difference method (FDM) for second-order in space and first-order in time was utilized to produce an approximation  $c_{approx}$  of  $c_{true}$ . Consequently, the network proposed by the study produces outcomes much more quickly than the FDM and outperforms the well-known approximation of Hagan et al. [8] in terms of accuracy. Nonetheless, McGhee only tries to make the predicted value  $c_{net}$  of the network come close to  $c_{approx}$ . In essence, the prediction error  $c_{net} - c_{true}$  is not considered in the study, and only the reduction of the fitting error  $c_{net} - c_{approx}$  is studied. Nevertheless,  $c_{net}$  should be close to  $c_{true}$  (i.e., not to  $c_{approx}$ ). Moreover, the research is not conducted systematically. We could not find any mentions about the number of epochs, the batch size, the weight initialization method, and the loss values for the training and test datasets. In particular, the types of neural networks tested in the research are fairly limited because the number of the hidden layers for the networks is fixed at one.

We believe that it is desirable to choose a parametric model without an exact pricing formula for vanilla options and investigate a training method of neural networks using numerous option prices for the model. Therefore, we decided to study the SABR model. Furthermore, a pricing method to generate big data should be efficient enough and easily applicable to a wide range of models, such as the rough volatility model [16]. Standard procedures satisfying the requirements may be the FDM and Monte-Carlo simulation (MC). Particularly, when the number of factors for underlying models is smaller than four, the FDM is usually more efficient and stable than the MC (see Wilmott [17]). This evidence denotes that the FDM may be more appropriate to price vanilla options under the SABR model than the MC because the model has two factors. Nevertheless, we chose the MC to produce  $c_{approx}$  because we think that neural networks have the potential to filter out symmetric noises caused by the MC, but they are unable to rectify the bias caused by the FDM. In other words, we do not choose the FDM but rather the MC because  $E[c_{approx}] = c_{true}$  for the MC case, but  $E[c_{approx}] \neq c_{true}$  for the FDM case. For example, Ferguson and Green [11] made two datasets using the MC, where one was precise but small, and the other was big yet imprecise, and they trained two networks with the datasets, respectively. Interestingly, the network using the larger and less precise dataset gives better results. This outcome indicates that the network can reduce the MC noises due to the integration of larger data. Thus, we also expect that the MC errors are reduced by a neural network provided the training data are sufficiently large.

Furthermore, based on nonlinear regression analysis, we propose a novel method to indirectly estimate the prediction error  $c_{net} - c_{true}$  even if  $c_{true}$  cannot be obtained. In other studies, the prediction error is usually expected to be greater than the approximation error  $c_{approx} - c_{true}$  because it is a sum of the approximation error and the fitting error  $c_{net} - c_{approx}$  that arises during training. However, neural networks are able to reduce a substantial part of the approximation error and produce  $c_{net}$  close to  $c_{true}$ . The method developed in this study would be an invaluable tool to evaluate the degree of the distance between  $c_{net}$  and  $c_{true}$ . When analyzing test results with the approach, the accuracy of our network is estimated to be comparable to that of about 13 million MC simulations.

Further, it is noticeable in the literature that although similar approaches are adopted for the same model, the loss of test data differ considerably depending on the details of the training methods. This notion is validated via the mean squared fitting errors (MSFE) of Culkin and Das [9], Broström and Kristiansson [10], Liu et al. [13], and Hirsra et al. [14] for the Black-Scholes model in Table 1 and 2. The MSFEs of Broström and Kristiansson and Liu et al. ( $7.27 \times 10^{-8}$  and  $8.21 \times 10^{-9}$ , respectively) seem to be superior to the MSFEs of Culkin and Das and Hirsra et al. ( $1.25 \times 10^{-4}$  and  $1.85 \times 10^{-5}$ , respectively). This association may be because the latter networks have narrower structures or learn from smaller data than the former. The former have 400 nodes per layer, and the latter have 100 or 140 nodes. Furthermore, the training data sizes of the former are 800 or 900 thousands, while the latter is 240 thousands. Either or both of the two options can facilitate performance gaps. These gaps can also be confirmed through the MSFEs for the Heston model of Liu et al. and Hirsra et al. ( $1.65 \times 10^{-8}$  and  $2.5 \times 10^{-5}$ , respectively). This notion implies that it is not easy to perfectly fit neural networks to the generated data. For a better goodness-of-fit, one should consider several factors, such as data size, network architecture, and the optimization method. Therefore, we try to reduce the MSFE in our experiment by generating enormous data and tuning various

hyperparameters for a considerably accurate fit.

In summary, this study contributes to the literature in the following ways. First, we generate numerous data using GPU-based simulations and verify that the network trained with the data provides extraordinarily accurate results. Second, we provide a novel method to analyze the prediction errors  $c_{net} - c_{true}$  by proposing an unbiased and consistent estimator associated with the prediction error. We make a new attempt using nonlinear regression, which forms the theoretical basis for the phenomenon that the network produces prediction errors smaller than the approximation errors  $c_{approx} - c_{true}$ .

The remainder of this paper is organized as follows. In Section 2, a new method of analyzing prediction errors with nonlinear regression is introduced. We then discuss the pricing methods of options in the SABR model and detailed methods of generating data for network learning in Section 3. In Section 4, we train neural networks of various structures and assess the impact of training data size on network performance. Finally, Section 5 concludes the study.

## 2. Nonlinear regression of numerous implied volatilities

As mentioned in the introduction, we only focus on the parametric models that do not have any exact pricing formulas. Therefore, an important step in this work is to generate numerous approximate implied volatilities  $\sigma_{approx,l}^I$  for exact volatilities  $\sigma_{true,l}^I$  ( $l = 1, 2, \dots, L$ ) under a parametric model, which will be used as the material to train networks. Each volatility  $\sigma_{approx,l}^I$  is generated on randomly chosen parameters, such as  $\theta_{l,1}, \theta_{l,2}, \dots, \theta_{l,n_\theta}$ , maturity  $T_l$ , and strike  $K_l$ .

As  $\sigma_{true,l}^I$  is determined by  $\theta_{l,1}, \theta_{l,2}, \dots, \theta_{l,n_\theta}, T_l$ , and  $K_l$ , there exists a function  $\tilde{h}$  such that  $\sigma_{true,l}^I = \tilde{h}(x_l)$  for  $x_l = (1, \theta_{l,1}, \theta_{l,2}, \dots, \theta_{l,n_\theta}, T_l, K_l)$ . According to the renowned universal approximation theorem, it is assumed that a network with enough number of weights  $\Gamma = \{\gamma_1, \gamma_2, \dots, \gamma_{n_\gamma}\}$  can accurately approximate the function value  $\tilde{h}(x_l)$  as its output  $h(x_l; \Gamma)$ . Thus, if  $M$  simulations are run to obtain the approximate volatility  $\sigma_{approx,l}^I$ , the central limit theorem yields the following relation:

$$\sigma_{approx,l}^I(M) = h(x_l; \Gamma) + \epsilon_l(M),$$

where  $\epsilon_l(M) \sim N(0, \beta_l^2/M)$  for  $\beta_l > 0$  (Glasserman [18]). Here, the time interval for the simulations is supposed to be small enough to neglect the bias of  $\sigma_{approx,l}^I$  against  $\sigma_{true,l}^I$ , and the notation  $\omega(M)$  is applied to emphasize that  $\omega$  is a random variable that is dependent on  $M$ .

In the perspective of nonlinear ordinary regression (Montgomery et al. [19]), an unbiased and consistent estimator  $\hat{\Gamma}$  of  $\Gamma$  is

$$\hat{\Gamma} = \underset{\Gamma}{\operatorname{argmin}} \mathcal{L}(\Gamma; M),$$

where

$$\mathcal{L}(\Gamma; M) = \frac{1}{2} \sum_{l=1}^L \left( h(x_l; \Gamma) - \sigma_{approx,l}^I(M) \right)^2.$$

The Jacobian and Hessian matrices  $J$  and  $H$  of  $\mathcal{L}(\hat{\Gamma}; M)$  should satisfy the optimality condition that  $J$  and  $H$  are zero and positive definite, respectively. On the other hand, we can derive

$$J = \epsilon Q, \quad H \approx Q^T Q, \tag{1}$$

(Hansen et al. [20]), where

$$\epsilon = [ \epsilon_1 \quad \epsilon_2 \quad \dots \quad \epsilon_L ], \quad Q = \begin{bmatrix} \frac{\partial h(x_1; \hat{\Gamma})}{\partial \gamma_1} & \frac{\partial h(x_1; \hat{\Gamma})}{\partial \gamma_2} & \dots & \frac{\partial h(x_1; \hat{\Gamma})}{\partial \gamma_{n_\gamma}} \\ \frac{\partial h(x_2; \hat{\Gamma})}{\partial \gamma_1} & \frac{\partial h(x_2; \hat{\Gamma})}{\partial \gamma_2} & \dots & \frac{\partial h(x_2; \hat{\Gamma})}{\partial \gamma_{n_\gamma}} \\ \vdots & \vdots & \ddots & \vdots \\ \frac{\partial h(x_L; \hat{\Gamma})}{\partial \gamma_1} & \frac{\partial h(x_L; \hat{\Gamma})}{\partial \gamma_2} & \dots & \frac{\partial h(x_L; \hat{\Gamma})}{\partial \gamma_{n_\gamma}} \end{bmatrix}.$$

Furthermore,  $\hat{\Gamma}$  follows a multivariate normal distribution as follows:

$$\hat{\Gamma} \sim N\left(\Gamma, \frac{1}{LM} \mathbf{W}^{-1} \mathbf{W}^\beta \mathbf{W}^{-1}\right),$$

where  $\mathbf{W} = \frac{1}{L} \mathbf{Q}^T \mathbf{Q}$ ,  $\mathbf{W}^\beta = \frac{1}{L} \mathbf{Q}^T \mathbf{B} \mathbf{Q}$ , and  $\mathbf{B}$  is the diagonal matrix with the  $l$ th diagonal entry  $\beta_l^2$ . Conversely, owing to the law of large numbers, the elements of  $\mathbf{W}$  and  $\mathbf{W}^\beta$  converge in probability to their respective expected values as  $L \rightarrow \infty$ . In other words,

$$\begin{aligned} \mathbf{W}_{k,k'} &= \left\langle \frac{\partial h(x_l; \hat{\Gamma}_M)}{\partial \gamma_k} \frac{\partial h(x_l; \hat{\Gamma}_M)}{\partial \gamma_{k'}} \right\rangle_{l,L} \xrightarrow{p} \left\langle \frac{\partial h(x_l; \hat{\Gamma}_M)}{\partial \gamma_k} \frac{\partial h(x_l; \hat{\Gamma}_M)}{\partial \gamma_{k'}} \right\rangle_l, \\ \mathbf{W}_{k,k'}^\beta &= \left\langle \beta_l^2 \frac{\partial h(x_l; \hat{\Gamma}_M)}{\partial \gamma_k} \frac{\partial h(x_l; \hat{\Gamma}_M)}{\partial \gamma_{k'}} \right\rangle_{l,L} \xrightarrow{p} \left\langle \beta_l^2 \frac{\partial h(x_l; \hat{\Gamma}_M)}{\partial \gamma_k} \frac{\partial h(x_l; \hat{\Gamma}_M)}{\partial \gamma_{k'}} \right\rangle_l \end{aligned}$$

as  $L \rightarrow \infty$ , where  $\langle \varphi_l \rangle_{l,L}$  and  $\langle \varphi_l \rangle_l$  are a sample mean of size  $L$  and the population mean of a random variable  $\varphi_l$ , respectively. That is,  $\langle \varphi_l \rangle_{l,L} = \frac{1}{L} \sum_{l=1}^L \varphi_l$ , and  $\langle \varphi_l \rangle_l = E[\varphi_l]$ . Notably,  $E[\langle \varphi_l \rangle_{l,L}] = \langle \varphi_l \rangle_l$ . Accordingly, if  $L \gg 1$ , then  $\mathbf{W}$  and  $\mathbf{W}^\beta$  rarely change, although  $L$  does change a little.

We now consider another dataset for an out-of-sample test, constituting  $L'$  volatilities  $\sigma_{approx,l}^I$  to approximate  $\sigma_{true,l}^I$  ( $l = 1, 2, \dots, L'$ ), each of which is generated from  $M'$  simulations. With regard to the dataset, the fitting error  $\epsilon_{fit,l}$ , the prediction error  $\epsilon_{pred,l}$ , and the approximation error  $\epsilon_{approx,l}$  are defined as follows:

$$\begin{aligned} \epsilon_{fit,l}(\hat{\Gamma}, M') &= \sigma_{net,l}^I(\hat{\Gamma}) - \sigma_{approx,l}^I(M'), \\ \epsilon_{pred,l}(\hat{\Gamma}) &= \sigma_{net,l}^I(\hat{\Gamma}) - \sigma_{true,l}^I, \quad \epsilon_{approx,l}(M') = \sigma_{approx,l}^I(M') - \sigma_{true,l}^I, \end{aligned}$$

where  $\sigma_{net,l}^I(\hat{\Gamma}) = h(x_l; \hat{\Gamma})$ . Notably,  $\epsilon_{pred,l}$  can be decomposed into  $\epsilon_{fit,l}$  and  $\epsilon_{approx,l}$ , that is,

$$\epsilon_{pred,l}(\hat{\Gamma}) = \epsilon_{fit,l}(\hat{\Gamma}, M') + \epsilon_{approx,l}(M').$$

Note that finding  $\epsilon_{fit,l}$  is straightforward while determining  $\epsilon_{pred,l}$  and  $\epsilon_{approx,l}$  is not simple because  $\sigma_{true,l}^I$  is unknown. Many researchers intuitively expect  $|\epsilon_{pred,l}| > |\epsilon_{approx,l}|$  because they guess that the signs of  $\epsilon_{fit,l}$  and  $\epsilon_{approx,l}$  are the same. Nonetheless, it would be the best if  $\epsilon_{fit,l}$  canceled out a part of  $\epsilon_{approx,l}$  so that  $|\epsilon_{pred,l}| < |\epsilon_{approx,l}|$ . This mechanism is possible only when the neural network can reduce the noises in  $\epsilon_{approx,l}$  and find more plausible values by itself. Specifically, we prove that self-correction of networks is feasible, and it will be demonstrated in the tests of Section 4.

Additionally, the errors  $\epsilon_{fit,l}$ ,  $\epsilon_{pred,l}$ , and  $\epsilon_{approx,l}$  follow their respective normal distributions as below:

$$\begin{aligned} \epsilon_{fit,l}(\hat{\Gamma}, M') &\sim N\left(0, \frac{\beta_l^2}{M'} + \frac{1}{LM} \mathbf{q}_l \mathbf{W}^{-1} \mathbf{W}^\beta \mathbf{W}^{-1} \mathbf{q}_l^T\right), \\ \epsilon_{approx,l}(M') &\sim N\left(0, \frac{\beta_l^2}{M'}\right), \quad \epsilon_{pred,l}(\hat{\Gamma}) \sim N\left(0, \frac{1}{LM} \mathbf{q}_l \mathbf{W}^{-1} \mathbf{W}^\beta \mathbf{W}^{-1} \mathbf{q}_l^T\right), \end{aligned} \quad (2)$$

where  $\mathbf{q}_l$  is the  $l$ th row vector of  $\mathbf{Q}$ . As mentioned above, it is extremely important to note that finding  $\epsilon_{pred,l}$  is infeasible because  $\sigma_{true,l}^I$  is unknown. This problem is serious because we need  $\epsilon_{pred,l}$  to evaluate the performance of the network. Although some might presume that the difficulty can be circumvented by computing  $\mathbf{Q}$ ,  $\mathbf{W}$ , and  $\mathbf{W}^\beta$ , the computation is severely unstable due to the countless parameters of the network.

To resolve the problem, we define three mean squared errors (MSE) for the test dataset, namely the mean squared fitting error  $\mathcal{E}_{fit}$ (MSFE), the mean squared prediction error  $\mathcal{E}_{pred}$  (MSPE), and the mean squared approximation error  $\mathcal{E}_{approx}$  (MSAE). They are given by the following:

$$\begin{aligned}\mathcal{E}_{fit}(\hat{\Gamma}, M'; L') &= \frac{1}{L'} \sum_{l=1}^{L'} \epsilon_{fit,l}^2(\hat{\Gamma}, M'), \\ \mathcal{E}_{pred}(\hat{\Gamma}; L') &= \frac{1}{L'} \sum_{l=1}^{L'} \epsilon_{pred,l}^2(\hat{\Gamma}), \quad \mathcal{E}_{approx}(M'; L') = \frac{1}{L'} \sum_{l=1}^{L'} \epsilon_{approx,l}^2(M').\end{aligned}$$

Among them, the MSPE  $\mathcal{E}_{pred}$  can serve as an indicator depicting the performance of the network with the weight  $\hat{\Gamma}$ . However, it also depends on the type of test set. Therefore, the following statistic will be utilized as an indicator to gauge performance:

$$\mathcal{E}_{pred}(\hat{\Gamma}) = E \left[ \mathcal{E}_{pred}(\hat{\Gamma}; L') \right],$$

which is the same as  $\langle \epsilon_{pred,l}^2(\hat{\Gamma}) \rangle_l$  because  $\mathcal{E}_{pred}(\hat{\Gamma}; L') = \langle \epsilon_{pred,l}^2(\hat{\Gamma}) \rangle_{l,L'}$ . We will explain the estimation of  $\mathcal{E}_{pred}(\hat{\Gamma})$  in the later sections. The propositions below describe the expectations and variances of  $\mathcal{E}_{fit}$ ,  $\mathcal{E}_{pred}$ , and  $\mathcal{E}_{approx}$ .

**Proposition 1.** *The expectations of  $\mathcal{E}_{fit}$ ,  $\mathcal{E}_{pred}$ , and  $\mathcal{E}_{approx}$  are given by*

$$\begin{aligned}E \left[ \mathcal{E}_{fit}(\hat{\Gamma}, M'; L') \right] &= E \left[ \mathcal{E}_{approx}(M'; L') \right] + E \left[ \mathcal{E}_{pred}(\hat{\Gamma}; L') \right], \\ E \left[ \mathcal{E}_{approx}(M'; L') \right] &= \frac{1}{M'} \langle \beta_l^2 \rangle_{l,L'}, \quad E \left[ \mathcal{E}_{pred}(\hat{\Gamma}; L') \right] = \frac{1}{LM} \langle \mathbf{q}_l \mathbf{W}^{-1} \mathbf{W}^\beta \mathbf{W}^{-1} \mathbf{q}_l^T \rangle_{l,L'}.\end{aligned}$$

*Proof.* As  $E \left[ \epsilon_{fit,l} \right] = 0$  for all  $l$ ,

$$\begin{aligned}E \left[ \mathcal{E}_{fit}(\hat{\Gamma}, M'; L') \right] &= \frac{1}{L'} \sum_{l=1}^{L'} \text{Var} \left[ \epsilon_{fit,l}(\hat{\Gamma}, M') \right] \\ &= \frac{1}{L'} \sum_{l=1}^{L'} \left( \frac{\beta_l^2}{M'} + \frac{1}{LM} \mathbf{q}_l \mathbf{W}^{-1} \mathbf{W}^\beta \mathbf{W}^{-1} \mathbf{q}_l^T \right) \\ &= \frac{1}{M'} \langle \beta_l^2 \rangle_{l,L'} + \frac{1}{LM} \langle \mathbf{q}_l \mathbf{W}^{-1} \mathbf{W}^\beta \mathbf{W}^{-1} \mathbf{q}_l^T \rangle_{l,L'}.\end{aligned}$$

Similarly,  $E \left[ \mathcal{E}_{approx} \right]$  and  $E \left[ \mathcal{E}_{pred} \right]$  are calculated as  $\frac{1}{M'} \langle \beta_l^2 \rangle_{l,L'}$  and  $\frac{1}{LM} \langle \mathbf{q}_l \mathbf{W}^{-1} \mathbf{W}^\beta \mathbf{W}^{-1} \mathbf{q}_l^T \rangle_{l,L'}$ , respectively.  $\square$

**Proposition 2.** *The variances of  $\mathcal{E}_{fit}$ ,  $\mathcal{E}_{pred}$ , and  $\mathcal{E}_{approx}$  are*

$$\begin{aligned}\text{Var} \left[ \mathcal{E}_{fit}(\hat{\Gamma}, M'; L') \right] &= \text{Var} \left[ \mathcal{E}_{approx}(M'; L') \right] + \text{Var} \left[ \mathcal{E}_{pred}(\hat{\Gamma}; L') \right] + \frac{4}{L'LM'M} \langle \beta_l^2 \mathbf{q}_l \mathbf{W}^{-1} \mathbf{W}^\beta \mathbf{W}^{-1} \mathbf{q}_l^T \rangle_{l,L'}, \\ \text{Var} \left[ \mathcal{E}_{approx}(M'; L') \right] &= \frac{2}{L'(M')^2} \langle \beta_l^4 \rangle_{l,L'}, \quad \text{Var} \left[ \mathcal{E}_{pred}(\hat{\Gamma}; L') \right] = \frac{2}{L'L^2M^2} \left\langle \left( \mathbf{q}_l \mathbf{W}^{-1} \mathbf{W}^\beta \mathbf{W}^{-1} \mathbf{q}_l^T \right)^2 \right\rangle_{l,L'}.\end{aligned}$$

*Proof.* The square  $X^2$  of a normal random variable  $X \sim N(0, \sigma^2)$  follows a gamma distribution  $\Gamma(1/2, 2\sigma^2)$ , which leads to

$$\epsilon_{fit,l}^2(\hat{\Gamma}, M') \sim \Gamma \left( \frac{1}{2}, 2 \left( \frac{\beta_l^2}{M'} + \frac{1}{LM} \mathbf{q}_l \mathbf{W}^{-1} \mathbf{W}^\beta \mathbf{W}^{-1} \mathbf{q}_l^T \right) \right).$$

As  $E[Y] = ab$  and  $Var[Y] = ab^2$  for  $Y \sim \Gamma(a, b)$ ,  $E[\epsilon_{fit,l}^2] = \frac{\beta_l^2}{M'} + \frac{1}{LM} \mathbf{q}_l \mathbf{W}^{-1} \mathbf{W}^\beta \mathbf{W}^{-1} \mathbf{q}_l^T$ , and  $Var[\epsilon_{fit,l}^2] = 2 \left( \frac{\beta_l^2}{M'} + \frac{1}{LM} \mathbf{q}_l \mathbf{W}^{-1} \mathbf{W}^\beta \mathbf{W}^{-1} \mathbf{q}_l^T \right)^2$ . As  $\epsilon_{fit,l}$  are independent,

$$\begin{aligned} & Var[\mathcal{E}_{fit}(\hat{\Gamma}, M'; L')] \\ &= \frac{1}{(L')^2} \sum_{l=1}^{L'} Var[\epsilon_{fit,l}^2(\hat{\Gamma}_M, M')] \\ &= \frac{1}{(L')^2} \sum_{l=1}^{L'} \left( \frac{2\beta_l^4}{(M')^2} + \frac{2}{L^2 M^2} (\mathbf{q}_l \mathbf{W}^{-1} \mathbf{W}^\beta \mathbf{W}^{-1} \mathbf{q}_l^T)^2 + \frac{4\beta_l^2}{LM'M} \mathbf{q}_l \mathbf{W}^{-1} \mathbf{W}^\beta \mathbf{W}^{-1} \mathbf{q}_l^T \right) \\ &= \frac{2}{L'(M')^2} \langle \beta_l^4 \rangle_{l,L'} + \frac{2}{L'L^2 M^2} \left\langle (\mathbf{q}_l \mathbf{W}^{-1} \mathbf{W}^\beta \mathbf{W}^{-1} \mathbf{q}_l^T)^2 \right\rangle_{l,L'} + \frac{4}{L'LM'M} \langle \beta_l^2 \mathbf{q}_l \mathbf{W}^{-1} \mathbf{W}^\beta \mathbf{W}^{-1} \mathbf{q}_l^T \rangle_{l,L'}. \end{aligned}$$

Similarly,  $Var[\mathcal{E}_{approx}]$  and  $Var[\mathcal{E}_{pred}]$  are derived as  $\frac{2}{L'(M')^2} \langle \beta_l^4 \rangle_{l,L'}$  and  $\frac{2}{L'L^2 M^2} \left\langle (\mathbf{q}_l \mathbf{W}^{-1} \mathbf{W}^\beta \mathbf{W}^{-1} \mathbf{q}_l^T)^2 \right\rangle_{l,L'}$ , respectively.  $\square$

Based on the propositions, the following theorem suggests an unbiased and consistent estimator of  $\mathcal{E}_{pred}(\hat{\Gamma})$ . The theorem needs two distinct test sets.

**Theorem 3.** *The estimator*

$$\hat{\mathcal{E}}_{pred}(\hat{\Gamma}) = \frac{M'_1 \mathcal{E}_{fit}(M'_1; L'_1) - M'_2 \mathcal{E}_{fit}(M'_2; L'_2)}{M'_1 - M'_2}$$

is unbiased and consistent to  $\mathcal{E}_{pred}(\hat{\Gamma})$  for  $M'_1 \neq M'_2$ . Particularly,  $(L'_1, L'_2)$  and  $(M'_1, M'_2)$  are the data lengths and the numbers of simulations for two distinct test sets, respectively. Further, the variance of  $\hat{\mathcal{E}}_{pred}(\hat{\Gamma})$  is given by

$$Var[\hat{\mathcal{E}}_{pred}(\hat{\Gamma})] = \left( \frac{M'_1}{M'_1 - M'_2} \right)^2 Var[\mathcal{E}_{fit}(\hat{\Gamma}_M, M'_1; L'_1)] + \left( \frac{M'_2}{M'_1 - M'_2} \right)^2 Var[\mathcal{E}_{fit}(\hat{\Gamma}_M, M'_2; L'_2)], \quad (3)$$

where

$$Var[\mathcal{E}_{fit}(\hat{\Gamma}, M'; L')] = \frac{2 \langle \beta_l^4 \rangle_{l,L'}}{L'(M')^2} + \frac{2 \left\langle (\mathbf{q}_l \mathbf{W}^{-1} \mathbf{W}^\beta \mathbf{W}^{-1} \mathbf{q}_l^T)^2 \right\rangle_{l,L'}}{L'L^2 M^2} + \frac{4 \langle \beta_l^2 \mathbf{q}_l \mathbf{W}^{-1} \mathbf{W}^\beta \mathbf{W}^{-1} \mathbf{q}_l^T \rangle_{l,L'}}{L'LM'M}.$$

*Proof.* The unbiasedness of  $\hat{\mathcal{E}}_{pred}(\hat{\Gamma})$  in relation to  $\mathcal{E}_{pred}(\hat{\Gamma})$  is exhibited as follows:

$$\begin{aligned} E[\hat{\mathcal{E}}_{pred}(\hat{\Gamma})] &= \frac{M'_1 E[\mathcal{E}_{fit}(M'_1; L'_1)] - M'_2 E[\mathcal{E}_{fit}(M'_2; L'_2)]}{M'_1 - M'_2} \\ &= \frac{\left( \langle \beta_l^2 \rangle_l + \frac{M'_1}{LM} \langle \mathbf{q}_l \mathbf{W}^{-1} \mathbf{W}^\beta \mathbf{W}^{-1} \mathbf{q}_l^T \rangle_l \right) - \left( \langle \beta_l^2 \rangle_l + \frac{M'_2}{LM} \langle \mathbf{q}_l \mathbf{W}^{-1} \mathbf{W}^\beta \mathbf{W}^{-1} \mathbf{q}_l^T \rangle_l \right)}{M'_1 - M'_2} \\ &= \frac{1}{LM} \langle \mathbf{q}_l \mathbf{W}^{-1} \mathbf{W}^\beta \mathbf{W}^{-1} \mathbf{q}_l^T \rangle_l = E[\mathcal{E}_{pred}(\hat{\Gamma}; L')] = \mathcal{E}_{pred}(\hat{\Gamma}). \end{aligned}$$

On the other hand, the form (3) for  $Var[\hat{\mathcal{E}}_{pred}(\hat{\Gamma})]$  is easily derived because  $\mathcal{E}_{fit}(M'_1; L'_1)$  and  $\mathcal{E}_{fit}(M'_2; L'_2)$  are independent of each other. Subsequently, by Proposition 2, because  $Var[\mathcal{E}_{fit}(M'_1; L'_1)]$  and  $Var[\mathcal{E}_{fit}(M'_2; L'_2)]$  converge to 0 as  $L_1$  and  $L_2$  go to infinity,  $\hat{\mathcal{E}}_{pred}(\hat{\Gamma})$  is consistent.  $\square$



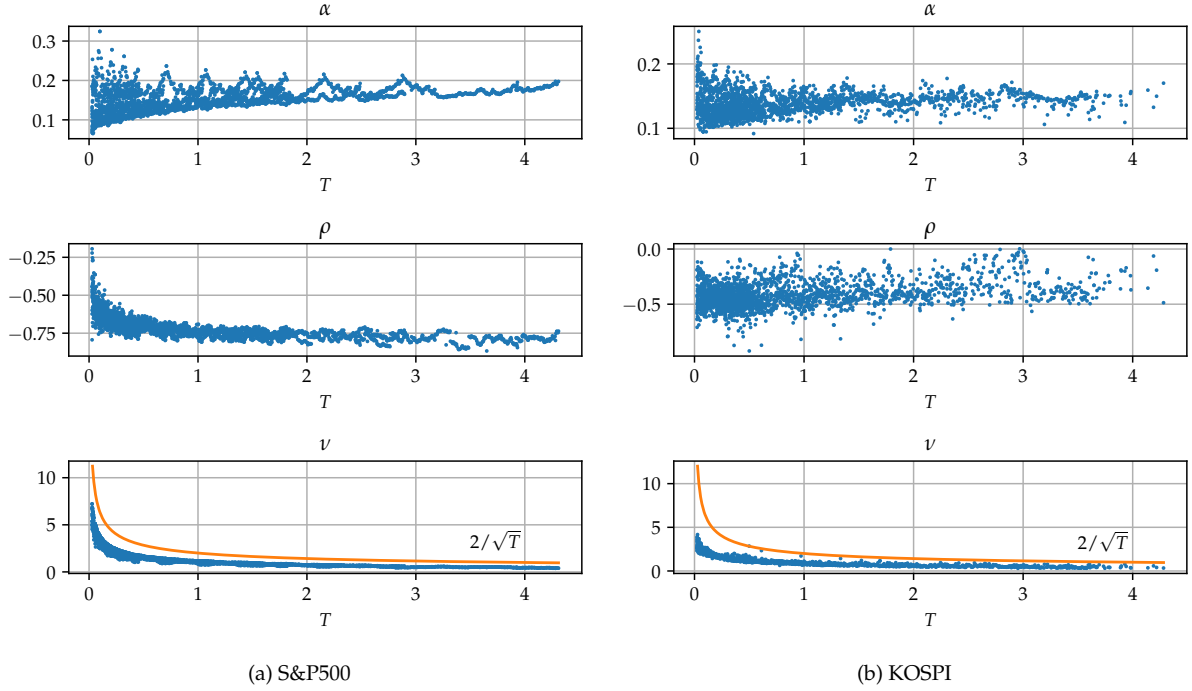


Figure 1: This figure shows the estimates of  $\alpha_0(T)$ ,  $\nu(T)$ , and  $\rho(T)$  for the SABR model where  $\beta(T) = 1$ . The values are obtained using the option data for the S&P 500 (left) and the KOSPI 200 (right) from April 2018 to March 2019.

When considering the theorem above,  $(M'_1, M'_2)$  and  $(L'_1, L'_2)$  should be set as  $M'_1 \gg M'_2$ ,  $L'_1 \gg 1$ , and  $L'_2 \gg 1$  to precisely estimate  $\mathcal{E}_{pred}(\hat{\Gamma})$ .

### 3. Data generation for network learning under the SABR model

#### 3.1. the SABR model

The SABR model [8] is expressed as the following stochastic differential equation (SDE):

$$\begin{aligned} df_t &= \alpha_t f_t^\beta dW_t, \\ d\alpha_t &= \nu \alpha_t dZ_t, \end{aligned}$$

where  $f_t$  is the forward price of an underlying asset (i.e., stock and interest rate) at time  $t$ , and  $W_t$  and  $Z_t$  are Brownian motions correlated with  $\rho \in (-1, 1)$ . The hidden state  $\alpha_t$  and the parameters  $\beta$ ,  $\rho$ ,  $\nu$  of the model have their respective roles in determining the shapes of implied volatility surface  $\sigma^I(T, K)$  (see Rebonato et al. [21] for a more detailed explanation). The state  $\alpha_t$  forms the backbone of the surface because the change of  $\alpha_t$  causes a parallel shift upward of the surface. The volatility of volatility parameter  $\nu$  handles the wings of the volatility surface because it controls the curvature of the surface. Conversely, the elasticity  $\beta$  and the correlation  $\rho$  play similar roles in adjusting the slopes of skews on the surface. Thus,  $\beta$  is commonly fixed as a constant from 0 to 1 to reduce model complexity. Aesthetic considerations result in  $\beta = 0$ ,  $\beta = 1/2$ , and  $\beta = 1$ , which are called the normal SABR, CIR (named after Cox, Ingersoll, and Ross) SABR, and the log-normal SABR, respectively. It is known that such arbitrary choices of  $\beta$  hardly ever decrease the fitting performance of the SABR model [22, 21]. Likewise, Bartlett [23] developed a hedging method less sensitive to particular values of  $\beta$ . From these studies, we choose the log-normal SABR ( $\beta = 1$ ) so that  $\alpha_t$  can be regarded as the volatility of  $f_t$ .

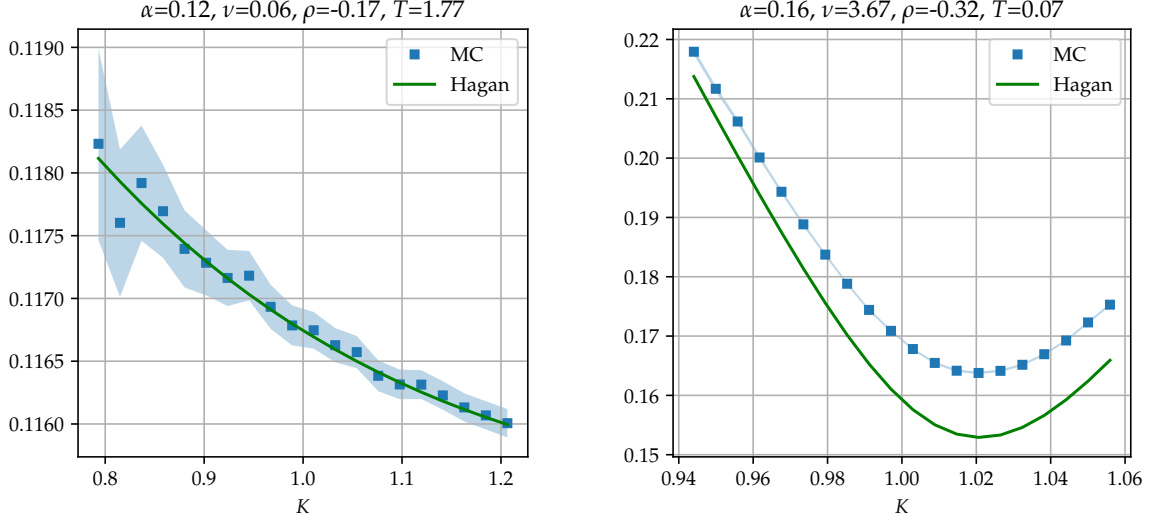


Figure 2: These figures are drawn to compare the implied volatilities provided by the Hagan formula (4) with the values of the MC. For the MC, we simulate 10 million paths for the time interval 0.002. The blue region indicates the 99% confidence interval for the MC.

The SABR model is mostly utilized as a fitting model to market volatilities by maturity, for which the state  $\alpha_0$  and parameters  $\beta$ ,  $\nu$ , and  $\rho$  are usually parameterized as  $\alpha_0(T)$ ,  $\beta(T)$ ,  $\nu(T)$ , and  $\rho(T)$ . Figure 1 displays the estimates of  $\alpha_0(T)$ ,  $\nu(T)$ , and  $\rho(T)$  when  $\beta(T) = 1$ . These are derived utilizing the option data for the S&P 500 (left) and the KOSPI 200 (right) from April 2018 to March 2019. The calibration is performed by Korean Asset Pricing, a bond rating agency located in Korea. From the figure, one can observe that all  $\alpha_0$  and  $\rho$  belong to  $(0.01, 0.5)$  and  $(-0.99, 0.1)$ , respectively, and all of  $\nu$  are lower than the baseline  $2/\sqrt{T}$ . Moreover, it seems that the values tend to become more unstable as  $T$  gets shorter, particularly for  $\nu$ . This association may result because the SABR model ignores short-term events such as fast-mean-reverting volatility.

Let us assume a fair price  $c$  for a vanilla option under the SABR model. Under the risk-neutral pricing framework [24], we can induce the pricing formula by solving the integral

$$c(t, K) = \int_0^\infty q(f_T; K) p_t(f_T) df_T,$$

or the partial differential equation (PDE)

$$\begin{aligned} \frac{\partial c}{\partial t} &= \frac{1}{2} \alpha^2 f^{2\beta} \frac{\partial^2 c}{\partial f^2} + \frac{1}{2} \nu^2 \alpha^2 \frac{\partial^2 c}{\partial \alpha^2} + \rho \nu \alpha^2 f^\beta \frac{\partial^2 c}{\partial f \partial \alpha}, \\ c(T, K) &= q(f_T; K), \end{aligned}$$

where  $p_t$  is the density of  $f_T$ ,  $K$  and  $T$  are the strike and maturity of the option, respectively, and  $q(\cdot; K)$  is the payoff function of the option with  $K$ . Regrettably, any exact pricing formulas cannot be derived for the option because the integral and the PDE are fairly hard to solve analytically. Instead, it is possible to derive a wide range of approximate formulas for the implied volatilities of the options [8, 25, 26, 27, 28, 29]. In fact, the aforementioned notion explains why the SABR model is so popular in practice.

Additionally, only for the case  $\beta = 1$ , we briefly mention the most well-known asymptotic formulas for the implied volatility  $\sigma^I$ , which was found by Hagan et al. [8] as follows:

$$\sigma^I(T, K) \approx \alpha_0 \frac{z}{\chi(z)} \left\{ 1 + \left[ \frac{1}{4} \rho \alpha_0 \nu + \frac{1}{24} (2 - 3\rho^2) \nu^2 \right] T \right\}, \quad (4)$$

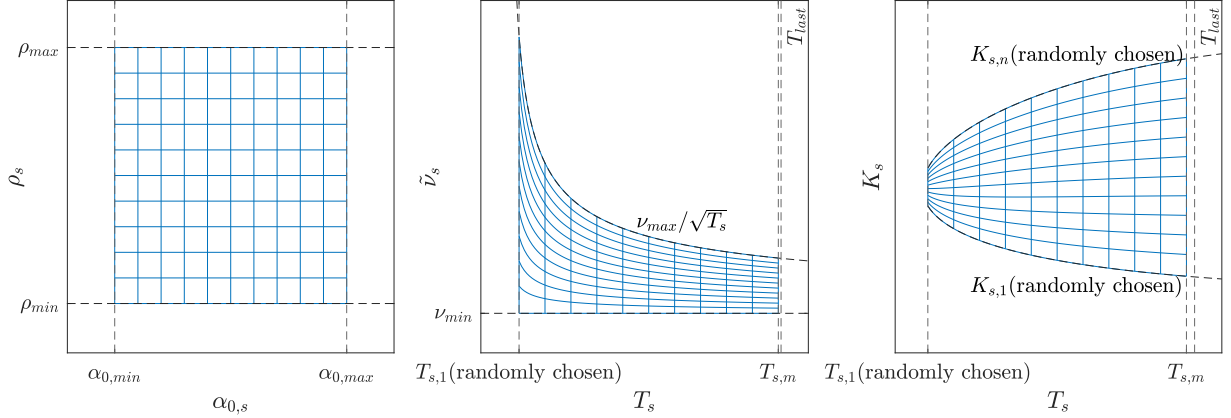


Figure 3: An illustration of the grid of  $\alpha_{0,s}$ ,  $\rho_s$ ,  $\tilde{v}_s$ ,  $K_s$ , and  $T_s$ .

where

$$z = \frac{\nu}{\alpha_0} \log \frac{f_0}{K}, \quad \chi(z) = \log \left\{ \frac{\sqrt{1 - 2\rho z + z^2} + z - \rho}{1 - \rho} \right\}.$$

As the above equations are derived using an asymptotic technique, it can be applied only for the option with a short maturity  $T$  and a strike  $K$  close to  $f_0$ . If one of the assumptions does not hold, this formula yields inexact prices, but even if all of the assumptions are satisfied, it does not always provide consistent accuracy. Figure 2 compares the implied volatilities formula with the MC-based values. Its accuracy is similar to that of the MC even when  $T$  is large (left), and vice versa (right). For the MC simulation, we simulate 10 million paths for the time interval 0.002. The blue region indicates the 99% confidence interval for the MC. Nevertheless, formula (4) is still popular due to its simplicity, especially in global over-the-counter interest rate derivatives market.

### 3.2. Data generation for network learning

In this subsection, we explain the method to generate extensive approximate implied volatilities  $\sigma_{approx,l}^I$  for exact implied volatilities  $\sigma_{true,l}^I$  ( $l = 1, \dots, L$ ) under the SABR model where  $\beta = 1$ , which will be used to train and test neural networks later. The volatilities  $\sigma_{approx,l}^I$  are grouped into  $mn$  data to form  $\tilde{L}$  surfaces  $\sigma_{approx,s}^I(T_{s,k_1}, K_{s,k_2})$ , with respect to  $T_{s,k_1}$  and  $K_{s,k_2}$ , where  $\tilde{L} = L/(mn)$ ,  $s = 1, \dots, \tilde{L}$ ,  $k_1 = 1, \dots, m$ , and  $k_2 = 1, \dots, n$ . In other words,  $L$  is the total number of generated data, and  $\tilde{L}$  is the number of volatility surfaces (a sort of partition of the data) with  $mn$  grid points.

When constructing grid points for the surfaces,  $K_{s,k_2}$  is set as a function of  $T_{s,k_1}$ ; that is,  $K_{s,k_2} = K_{s,k_2}(T_{s,k_1})$ . This mechanism is intended to widen the width of strike range  $[K_{s,1}, K_{s,n}]$  as  $T_{s,k_1}$  gets larger, in other words,

$$\log \frac{K_{s,n}}{f_{0,s}} - \log \frac{K_{s,1}}{f_{0,s}} \propto \text{std} \left[ \log \frac{f_{T_{s,k_1},s}}{f_{0,s}} \right],$$

where  $f_{t,s}$  is the forward price at  $t$  under the parameters  $\alpha_{0,s}$ ,  $\tilde{v}_s$  ( $:= \nu_s / \sqrt{T_{s,k_1}}$ ), and  $\rho_s$ . Note that the parameter  $\tilde{v}_s$  depends on  $T_{s,k_1}$ . As mentioned before, practitioners usually fit the SABR model to the market data  $\sigma^I(T)$  for each maturity  $T$  separately. If so, as shown in Figure 1, the estimates of  $\nu$  tend to get larger as  $T$  becomes shorter in market data. Hence,  $\tilde{v}_s$  is set up in a way to capture the phenomenon.

Let us explain the construction process of the grid points in more detail. Suppose that data is generated until the time  $T_{last}$ . The maturity  $T_{s,k_1}$  and strike  $K_{s,k_2}$  for the  $s$ th surface  $\sigma_{approx,s}^I(T_{s,k_1}, K_{s,k_2})$  are randomly chosen as follows:

1. Set a time grid interval  $\Delta T = T_{last}/m$ , initialize the first time point  $T_{s,1}$  randomly in  $(0, \Delta T]$ , and choose the other points equidistantly by  $T_{s,k_1} = T_{s,1} + (k_1 - 1) \Delta T$ .
2. Determine the start point  $K_{s,1}$  and the end point  $K_{s,n}$  of  $K_s$ -range by the formula

$$K_{s,1} = f_{0,s} \exp \left( -\frac{1}{2} \frac{\alpha_{0,s}}{\tilde{v}_s^2} \left( \exp \left\{ \tilde{v}_s^2 T_{s,k_1} \right\} - 1 \right) - \eta_f \frac{\alpha_{0,s}}{\tilde{v}_s} \left( \exp \left\{ \tilde{v}_s^2 T_{s,k_1} \right\} - 1 \right)^{1/2} \right),$$

$$K_{s,n} = f_{0,s} \exp \left( -\frac{1}{2} \frac{\alpha_{0,s}^2}{\tilde{v}_s^2} \left( \exp \left\{ \tilde{v}_s^2 T_{s,k_1} \right\} - 1 \right) + \eta_f \frac{\alpha_{0,s}}{\tilde{v}_s} \left( \exp \left\{ \tilde{v}_s^2 T_{s,k_1} \right\} - 1 \right)^{1/2} \right),$$

where  $\eta_f$  follows the uniform distribution  $U(0.842, 2.576)$ , and the hidden state  $\alpha_{0,s}$  and parameters  $v_s$  (not  $\tilde{v}_s$ ) and  $\rho_s$  are also sampled uniformly within predetermined limits. That is,

$$\alpha_{0,s} \sim U(\alpha_{0,min}, \alpha_{0,max}), \quad v_s \sim U(v_{min}, v_{max}), \quad \rho_s \sim U(\rho_{min}, \rho_{max}).$$

3. Equidistantly partition the interval  $[K_{s,1}, K_{s,n}]$  for each  $T_{s,k_1}$  by  $K_{s,k_2} = K_{s,1} + (k_2 - 1) \Delta K$ , where  $\Delta K = (K_{s,n} - K_{s,1})/n$ .

If the number  $\tilde{L}$  of the surfaces is reasonably large, the random numbers  $\{(\alpha_{0,s}, v_s, \rho_s) : s = 1, \dots, \tilde{L}\}$  may fill most of the parameter space  $\{\alpha_{0,min} \leq \alpha_0 \leq \alpha_{0,max}\} \times \{v_{min} \leq v \leq v_{max}\} \times \{\rho_{min} \leq \rho \leq \rho_{max}\}$  evenly and densely. In addition, we suppose  $f_{0,s} = 1$  without loss of generality. Note that  $f_{t,s}$  of the SABR model where  $\beta = 1$  can be expressed as  $d(f_{t,s}/f_{0,s}) = \alpha_{t,s}(f_{t,s}/f_{0,s}) dW_t$ . This notion implies that an option price  $c$  is homogeneous of degree one in both  $f_{0,s}$  and  $K$  under the SABR model, that is,  $c = c(K/f_{0,s})$  (Garcia and Gençay [30]), which supports the assumption  $f_{0,s} = 1$ . Figure 3 is an illustration of the grids  $\alpha_{0,s}$ ,  $\rho_s$ ,  $\tilde{v}_s$ ,  $K_s$ , and  $T_s$ . The grid for  $\alpha_0$  and  $\rho$  is partitioned evenly, the partition  $\{T_{s,k_1}\}$  is chosen randomly, but  $T_{s,1}$  cannot be less than 0, and  $T_{s,m}$  cannot be greater than  $T_{last}$ . The upper boundary of  $\tilde{v}_s$  is dependent on  $T_{s,k_1}$  because  $\tilde{v}_s = v_{max}/\sqrt{T_{s,k_1}}$ , where  $v_{max}$  is selected based on Figure 1. The strike boundary also relies on  $T_{s,k_1}$ , and it widens and narrows under the influence of the value of the random variable  $\eta_f$ . All grid points inside the boundaries are split equidistantly.

To obtain the approximate implied volatility  $\sigma_{approx,s}^I(T_{s,k_1}, K_{s,k_2})$ , we simulate  $N$  paths of the SABR model ( $\beta = 1$ ) under the parameters  $(\alpha_{0,s}, \tilde{v}_s, \rho_s)$  using the Monte-Carlo Euler scheme, which can be expressed as follows:

$$f_{t+\Delta t,s} = f_{t,s} + \alpha_{t,s} f_{t,s} \left( e_{t,s} \sqrt{\Delta t} \right),$$

$$\alpha_{t+\Delta t,s} = \alpha_{t,s} + \tilde{v}_s \alpha_{t,s} \left( \rho_s e_{t,s} \sqrt{\Delta t} + \sqrt{1 - \rho_s^2} \tilde{e}_{t,s} \sqrt{\Delta t} \right),$$

where  $t = \Delta t, 2\Delta t, \dots, T_{s,m} - \Delta t$ ,  $f_{0,s} = 1$ , and  $(e_{t,s}, \tilde{e}_{t,s})$  are independent standard normal random variables. Further, the MC gives an approximate price  $c_{approx,s,k_1,k_2}$  for the true option price  $c_{true,s,k_1,k_2}$  under the SABR model in the following way:

$$c_{approx,s,k_1,k_2} = \frac{1}{N} \sum_{j=1}^N c_{approx,s,k_1,k_2,j} = \frac{1}{N} \sum_{j=1}^N q \left( f_{T_{s,k_1},s,j}, K_{s,k_2} \right),$$

where the subscript  $j$  represents that the value originated from the  $j$ th path, and  $q(\cdot; K_{s,k_2})$  is the option payoff for strike  $K_{s,k_2}$ . Price  $c_{approx,s,k_1,k_2}$  is then converted to its implied volatility  $\sigma_{approx,s,k_1,k_2}^I$ . We use Powell's method to obtain the implied volatility by minimizing  $(BS(\sigma_{approx,s,k_1,k_2}^I) - c_{approx,s,k_1,k_2})^2$ , where  $BS(\sigma)$  is the Black-Scholes formula for the option. In this process, we only utilize out-of-the-money (OTM) call and put options. The price of OTM call options explodes occasionally. Therefore, if the standard deviation of the simulations exceeds by 100 times the average, the data were excluded from the experiment (approximately 3.6% of the data are excluded in this manner).

dataset	$N$ (# of paths)	$\tilde{L}$ (# of surface)	$L$ (# of total data)
training set ( $\mathcal{D}_{train}$ )	500k	1.2M	480M
validation set ( $\mathcal{D}_{validate}$ )	500k	0.1M	40M
test set ( $\mathcal{D}_{test}$ )	500k	0.1M	40M
more accurate set ( $\mathcal{D}'_{test}$ )	12.5M	0.25M	100M
total		1.65M	660M

Table 3: This table displays the datasets for our experiments, which contain approximate implied volatilities  $\sigma_{approx,l}^I$  for  $\sigma_{true,l}^I$  ( $l = 1, \dots, L$ ). They are generated by the MC with  $N$  paths for a time interval of 0.002. Furthermore,  $\sigma_{approx,l}^I$  are grouped to form  $\tilde{L}$  surfaces. The symbols "k" and "M" indicate one thousand and one million, respectively.

The hyperparameters are chosen as follows:  $m = 20$ ,  $n = 20$ ,  $\alpha_{0,min} = 0.01$ ,  $\alpha_{0,max} = 0.5$ ,  $\nu_{min} = 0.01$ ,  $\nu_{max} = 2$ ,  $\rho_{min} = -0.99$ ,  $\rho_{max} = 0.1$ , and  $T_{last} = 2$ . With the hyperparameters, we separately make 1.2M surfaces ( $N = 5E + 5$ ,  $L = 4.8E + 8$ ) for training, 0.1M surfaces ( $N = 5E + 5$ ,  $L = 4E + 7$ ) for a validation, 0.1M surfaces for a test with simulation accuracy  $\Delta t = 0.002$  and  $N = 5E + 5$ . In fact, we generate 250k paths with the antithetic variate method in the experiment, but it is known that this approach is superior to when 500k paths are generated without the method. Moreover, we create 0.25M surfaces with a higher accuracy  $N = 1.25E + 7$  ( $L = 1E + 8$ ) while keeping  $\Delta t$  as 0.002. These additional data are employed for error analysis, which will be explained in the following section. For convenience, the four kinds of datasets are summarized in Table 3. Contrarily, to generate the datasets, we performed the MC in parallel using many GPUs (GeForce GTX 1080 TI  $\times 8$ , GeForce RTX 2080 TI  $\times 16$ , Tesla V100  $\times 2$ ). Despite using many GPUs, the procedure took about a month to complete.

#### 4. Network-based prediction of implied volatilities

In this section, we train neural networks of various structures using the training dataset  $\mathcal{D}_{train}$  and the validation dataset  $\mathcal{D}_{validate}$ . Subsequently, we predict the data in the test dataset  $\mathcal{D}_{test}$  with the best-performing network among them. We also predict the data in the more accurate test dataset  $\mathcal{D}'_{test}$  to evaluate the networks by estimating  $\mathcal{E}_{pred}(\hat{\Gamma})$  with Theorem 3 in Section 2. In addition, new notations are introduced confirming that  $\mathcal{E}_{fit}(\hat{\Gamma}, \mathcal{D}) = \mathcal{E}_{fit}(\hat{\Gamma}, M'; L')$ ,  $\mathcal{E}_{pred}(\hat{\Gamma}; \mathcal{D}) = \mathcal{E}_{pred}(\hat{\Gamma}; L')$ ,  $\mathcal{E}_{approx}(\mathcal{D}) = \mathcal{E}_{approx}(M'; L')$ ,  $\mathcal{N}_{pred}(\hat{\Gamma}, \mathcal{D}) = \mathcal{N}_{pred}(\hat{\Gamma}, M'; L')$  for the dataset  $\mathcal{D}$  with data length  $L'$  for  $M'$  simulations (i.e., see below for the definition of  $\mathcal{N}_{pred}$ ). The notations are used when it is desirable to emphasize  $\mathcal{D}$  more than  $L'$  and  $M'$  in the context.

The expected number  $\mathcal{N}_{pred}$  of virtual simulations to achieve  $\mathcal{E}_{pred}(\hat{\Gamma})$  is defined as follows:

$$\mathcal{N}_{pred}(\hat{\Gamma}, M'; L') = M' \frac{\mathcal{E}_{fit}(\hat{\Gamma}, M'; L') - \mathcal{E}_{pred}(\hat{\Gamma})}{\mathcal{E}_{pred}(\hat{\Gamma})}, \quad (5)$$

which is utilized as an indicator of the network performance, along with  $\mathcal{E}_{pred}(\hat{\Gamma})$ . The definition is plausible because  $\mathcal{E}_{approx}(M'; L') = \mathcal{E}_{fit}(\hat{\Gamma}, M'; L') - \mathcal{E}_{pred}(\hat{\Gamma}; L')$ , and it is expected that  $|\mathcal{E}_{pred}(\hat{\Gamma}) - \mathcal{E}_{pred}(\hat{\Gamma}; L')|$  is considerably small. For instance, suppose that  $\mathcal{N}_{pred}$  is approximately one million. This supposition implies that simulations should be performed one million times so that the MC can attain the accuracy of the network.

We use an extensive feedforward neural network with millions of weights. By increasing network size when possible, we expect that approximation capability will be maximized. It accepts the following five

# of nodes	$\mathcal{E}_{pred}(\hat{\Gamma})$				$\mathcal{N}_{pred}(\hat{\Gamma}, \mathcal{D}_{test})$			
	# of layers				# of layers			
	4	5	6	7	4	5	6	7
3,000	2.22E-7	2.13E-7	2.27E-7	2.04E-7	11.80M	12.31M	11.52M	12.84M
5,000	2.23E-7	2.05E-7	2.05E-7	2.03E-7	11.73M	12.81M	12.81M	12.88M
7,000	<b>2.03E-7</b>	2.10E-7	2.06E-7	2.06E-7	<b>12.95M</b>	12.50M	12.71M	12.72M

Table 4: This table denotes the values of the two indicators of network performance,  $\mathcal{E}_{pred}(\hat{\Gamma})$  and  $\mathcal{N}_{pred}(\hat{\Gamma}, \mathcal{D}_{test})$ , for various network structures ("M" indicates one million).

inputs

$$\begin{aligned}
T_s &= \begin{bmatrix} T_{s,1} & T_{s,1} & \cdots & T_{s,1} \\ T_{s,2} & T_{s,2} & \cdots & T_{s,2} \\ \vdots & \vdots & \ddots & \vdots \\ T_{s,m} & T_{s,m} & \cdots & T_{s,m} \end{bmatrix}, \quad K_s = \begin{bmatrix} K_{s,1,1} & K_{s,1,2} & \cdots & K_{s,1,n} \\ K_{s,2,1} & K_{s,2,2} & \cdots & K_{s,2,n} \\ \vdots & \vdots & \ddots & \vdots \\ K_{s,m,1} & K_{s,m,2} & \cdots & K_{s,m,n} \end{bmatrix}, \\
\alpha_{0,s} &= \begin{bmatrix} \alpha_{0,s} & \alpha_{0,s} & \cdots & \alpha_{0,s} \\ \alpha_{0,s} & \alpha_{0,s} & \cdots & \alpha_{0,s} \\ \vdots & \vdots & \ddots & \vdots \\ \alpha_{0,s} & \alpha_{0,s} & \cdots & \alpha_{0,s} \end{bmatrix}, \quad \mathbf{v}_s = \begin{bmatrix} v_s & v_s & \cdots & v_s \\ v_s & v_s & \cdots & v_s \\ \vdots & \vdots & \ddots & \vdots \\ v_s & v_s & \cdots & v_s \end{bmatrix}, \quad \boldsymbol{\rho}_s = \begin{bmatrix} \rho_s & \rho_s & \cdots & \rho_s \\ \rho_s & \rho_s & \cdots & \rho_s \\ \vdots & \vdots & \ddots & \vdots \\ \rho_s & \rho_s & \cdots & \rho_s \end{bmatrix},
\end{aligned}$$

where  $K_{s,k_1,k_2} = K_{s,k_2}(T_{s,k_1})$ , and produces the following SABR volatilities:

$$\sigma_{net,s}^I = \begin{bmatrix} \sigma_{net,s}^I(T_{s,1}, K_{s,1,1}, \alpha_{0,s}, v_s, \rho_s) & \cdots & \sigma_{net,s}^I(T_{s,1}, K_{s,1,n}, \alpha_{0,s}, v_s, \rho_s) \\ \vdots & \ddots & \vdots \\ \sigma_{net,s}^I(T_{s,m}, K_{s,m,1}, \alpha_{0,s}, v_s, \rho_s) & \cdots & \sigma_{net,s}^I(T_{s,m}, K_{s,m,n}, \alpha_{0,s}, v_s, \rho_s) \end{bmatrix}.$$

It is worthy to recall that  $\sigma_{approx,s}^I$  ( $s = 1, 2, \dots, \tilde{L}$ ) is also generated as a two-dimensional form via

$$\sigma_{approx,s}^I = \begin{bmatrix} \sigma_{approx,s}^I(T_{s,1}, K_{s,1,1}, \alpha_{0,s}, v_s, \rho_s) & \cdots & \sigma_{approx,s}^I(T_{s,1}, K_{s,1,n}, \alpha_{0,s}, v_s, \rho_s) \\ \vdots & \ddots & \vdots \\ \sigma_{approx,s}^I(T_{s,m}, K_{s,m,1}, \alpha_{0,s}, v_s, \rho_s) & \cdots & \sigma_{approx,s}^I(T_{s,m}, K_{s,m,n}, \alpha_{0,s}, v_s, \rho_s) \end{bmatrix}.$$

This kind of approach would help a network in filtering out simulation noises by checking adjacent values. Dimitroff et al. [31] and Bayer et al. [32] adopted similar approaches.

The optimal weights  $\hat{\Gamma}$  are determined by minimizing the sum of squared differences between  $\sigma_{net,s}^I$  with  $\sigma_{approx,s}^I$  in  $\mathcal{D}_{train}$ . To this end, the adaptive moment estimation (ADAM, Kingma and Ba [33]) is used with the batch size 100. The learning rate is initially set to be  $1e^{-5}$ , but it is reduced by a factor of 10 every time the loss value for  $\mathcal{D}_{validate}$  is not improved. When the learning rate reaches the value  $1e^{-8}$ , the training is finished. We refer to Liu et al. [13] for the configuration.

We train and test various structures of the network while varying the numbers of layers and nodes per each hidden layer. Table 4 reveals  $\mathcal{E}_{pred}(\hat{\Gamma})$  and  $\mathcal{N}_{pred}(\hat{\Gamma}, \mathcal{D}_{test})$  for the networks, which are induced using Theorem 3 with  $\mathcal{E}_{fit}(\hat{\Gamma}, \mathcal{D}_{test})$  and  $\mathcal{E}_{fit}(\hat{\Gamma}, \mathcal{D}'_{test})$ . In addition,  $\mathcal{E}_{pred}(\hat{\Gamma})$  are spread from  $2.03 \times 10^{-7}$  to  $2.22 \times 10^{-7}$ , and  $\mathcal{N}_{pred}(\hat{\Gamma}, \mathcal{D}_{test})$  are distributed from 11.52M to 12.95M ("M" indicates one million). After observing the figures on the table, we conclude that there are no significant differences between the performances of the networks. However, notably, the values tend to improve slightly as the numbers of layers and nodes increase. We chose the network with 4 layers and 7,000 nodes as the best performance network. Thus, we will only continue subsequent tests for the chosen network.

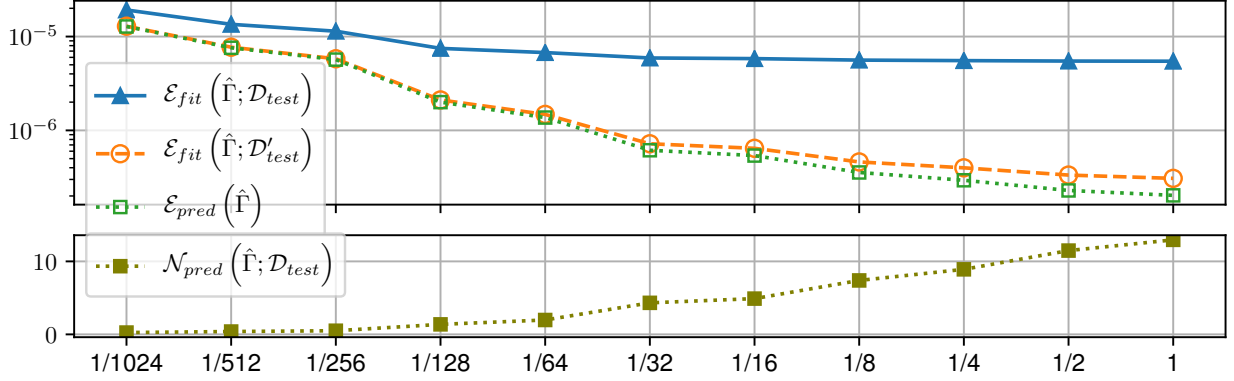


Figure 4: This figure draws  $\mathcal{E}_{fit}(\hat{\Gamma}, \mathcal{D}_{test})$ ,  $\mathcal{E}_{fit}(\hat{\Gamma}, \mathcal{D}'_{test})$ ,  $\mathcal{E}_{pred}(\hat{\Gamma})$ , and  $\mathcal{N}_{pred}(\hat{\Gamma}, \mathcal{D}_{test})$  with respect to training data size.

Subsequently, we analyze the effect of training data size  $L$  on network performance. Figure 4 draws  $\mathcal{E}_{fit}(\hat{\Gamma}, \mathcal{D}_{test})$ ,  $\mathcal{E}_{fit}(\hat{\Gamma}, \mathcal{D}'_{test})$ ,  $\mathcal{E}_{pred}(\hat{\Gamma})$ , and  $\mathcal{N}_{pred}(\hat{\Gamma}, \mathcal{D}_{test})$  with respect to  $L$ . To obtain the values, training and test are repeated using part of the training set  $\mathcal{D}_{train}$ . For instance, the values for the "1/128" subset originate from the network trained by only using 1/128 part of  $\mathcal{D}_{train}$ . A subset contains other subsets with smaller sizes. For example, the subset "1/256" contains the subset "1/512", and the subset "1/512" contains the subset "1/1024". In the figure,  $\mathcal{E}_{fit}(\hat{\Gamma}, \mathcal{D}_{test})$ ,  $\mathcal{E}_{fit}(\hat{\Gamma}, \mathcal{D}'_{test})$ , and  $\mathcal{E}_{pred}(\hat{\Gamma})$  decrease, and  $\mathcal{N}_{pred}(\hat{\Gamma})$  increases as the training data size  $L$  increases. This phenomenon can be understood through Proposition 1 and Theorem 3. Accordingly, it is established that

$$E[\mathcal{E}_{fit}(\hat{\Gamma}, \mathcal{D})] = E[\mathcal{E}_{pred}(\hat{\Gamma}; \mathcal{D})] + E[\mathcal{E}_{approx}(\mathcal{D})] = \frac{1}{LM} \langle \mathbf{q}_l \mathbf{W}^{-1} \mathbf{W}^\beta \mathbf{W}^{-1} \mathbf{q}_l^T \rangle_{l, L'} + \frac{1}{M'} \langle \beta_l^2 \rangle_{l, L'},$$

$$E[\mathcal{E}_{pred}(\hat{\Gamma})] = \frac{1}{LM} \langle \mathbf{q}_l \mathbf{W}^{-1} \mathbf{W}^\beta \mathbf{W}^{-1} \mathbf{q}_l^T \rangle_{l, L'}, \quad E[\mathcal{N}_{pred}(\hat{\Gamma}; \mathcal{D})] = \frac{LM}{M'} \langle \beta_l^2 \rangle_{l, L'} \langle \mathbf{q}_l \mathbf{W}^{-1} \mathbf{W}^\beta \mathbf{W}^{-1} \mathbf{q}_l^T \rangle_{l, L'}^{-1}$$

for the dataset  $\mathcal{D}$  with data length  $L'$  for  $M'$  simulations ( $M$  is the number of simulations to generate the data in  $\mathcal{D}_{train}$ ). By the formulas above,  $\mathcal{E}_{pred}(\hat{\Gamma}; \mathcal{D})$  is reduced with a high probability as  $L$  increases, but  $\mathcal{E}_{approx}(\mathcal{D})$  is independent of  $L$ . Thus, as the training data size  $L$  grows,  $\mathcal{E}_{fit}(\hat{\Gamma}, \mathcal{D})$  probably decreases and converges to  $\mathcal{E}_{app}(\mathcal{D})$ . It also seems reasonable that  $\mathcal{E}_{pred}(\hat{\Gamma})$  and  $\mathcal{N}_{pred}(\hat{\Gamma}; \mathcal{D})$  monotonically decrease and increase, respectively. Nonetheless, according to the formulas above,  $\mathcal{E}_{pred}(\hat{\Gamma})$  and  $\mathcal{N}_{pred}(\hat{\Gamma}; \mathcal{D})$  should approximately be half and doubled, respectively. Nevertheless, in the graphs, the decrease rate of  $\mathcal{E}_{pred}(\hat{\Gamma})$  is higher than 0.5, and the increase rate of  $\mathcal{N}_{pred}(\hat{\Gamma}; \mathcal{D})$  is lower than 2. These results may be because the optimal weights  $\hat{\Gamma}$  are all different depending on the training data size  $L$ , highlighting that matrices such as  $\mathbf{W}$  and  $\mathbf{W}^\beta$  adjust if  $L$  changes. Further, we guess that the approximation of the Hessian for the loss function in (1) leads to these outcomes. We leave this issue for future endeavors.

We further investigate  $\mathcal{E}_{pred}(\hat{\Gamma})$  and  $\mathcal{N}_{pred}(\hat{\Gamma}, \mathcal{D}_{test})$  while restricting the range of one of the inputs  $\alpha_0$ ,  $\nu$ ,  $\rho$ ,  $K$ , and  $T$ . Thus, let  $[Q_k, Q_{k+1}]$  be a subset containing the bottom 20% to 20(k+1)% of a given set. Recall that  $\alpha_0$  is generated to be uniformly distributed from 0 to 2 (if exactly speaking, from 0.01 to 2). Thus,  $[Q_k, Q_{k+1}]$  for  $\alpha_0$  is  $\{\alpha_0 | \frac{2}{5}k \leq \alpha_0 \leq \frac{2}{5}(k+1)\}$ . Table 5 illustrates how  $\mathcal{E}_{pred}(\hat{\Gamma})$  and  $\mathcal{N}_{pred}(\hat{\Gamma}, \mathcal{D}_{test})$  change when one of the inputs is restricted into  $[Q_k, Q_{k+1}]$ . In the lower table,  $[Q_0, Q_5]$  represents that any restriction for the inputs is not imposed. Evidently,  $\mathcal{N}_{pred}(\hat{\Gamma}, \mathcal{D}_{test})$  is large concerning specific domains (e.g.,  $[Q_4, Q_5]$  for  $\alpha_0$ ). The large  $\mathcal{N}_{pred}(\hat{\Gamma}, \mathcal{D}_{test})$  means that  $\mathcal{E}_{fit}(\hat{\Gamma}, \mathcal{D}_{test}) / \mathcal{E}_{pred}(\hat{\Gamma})$  is also high (see equation (5)). As  $\mathcal{E}_{pred}(\hat{\Gamma})$  positively correlates with  $\mathcal{N}_{pred}(\hat{\Gamma}, \mathcal{D}_{test})$  in the table, this correlation leads to the fact that the domains with large  $\mathcal{N}_{pred}(\hat{\Gamma}, \mathcal{D}_{test})$  have greater  $\mathcal{E}_{fit}(\hat{\Gamma}, \mathcal{D}_{test})$ . Therefore, we conclude that the network reduces more noises in those domains where  $\mathcal{E}_{fit}(\hat{\Gamma}, \mathcal{D}_{test})$  is high. The phenomenon may occur because

	$\alpha_0$		$\nu$		$\rho$		$K$		$T$	
	$\mathcal{E}_{pred}$	$\mathcal{N}_{pred}$	$\mathcal{E}_{pred}$	$\mathcal{N}_{pred}$	$\mathcal{E}_{pred}$	$\mathcal{N}_{pred}$	$\mathcal{E}_{pred}$	$\mathcal{N}_{pred}$	$\mathcal{E}_{pred}$	$\mathcal{N}_{pred}$
[Q <sub>0</sub> , Q <sub>1</sub> ]	2.1E-8	4.2M	1.7E-8	7.5M	5.8E-7	11.7M	2.7E-8	12.3M	1.8E-7	15.3M
[Q <sub>1</sub> , Q <sub>2</sub> ]	7.0E-8	9.4M	2.2E-8	11.0M	2.8E-7	12.6M	2.2E-8	9.6M	2.1E-7	12.8M
[Q <sub>2</sub> , Q <sub>3</sub> ]	1.6E-7	11.9M	1.1E-7	10.1M	8.9E-8	17.5M	2.9E-7	6.7M	2.1E-7	12.6M
[Q <sub>3</sub> , Q <sub>4</sub> ]	3.0E-7	12.6M	4.2E-7	9.5M	3.5E-8	18.5M	4.2E-7	10.4M	2.1E-7	12.1M
[Q <sub>4</sub> , Q <sub>5</sub> ]	4.7E-7	13.9M	5.4E-7	15.0M	4.2E-8	6.6M	3.1E-7	22.2M	2.1E-7	12.1M

	$\mathcal{E}_{pred}$	$\mathcal{N}_{pred}$
[Q <sub>0</sub> , Q <sub>5</sub> ]	2.03E-7	12.95M

Table 5: The table shows  $\mathcal{E}_{pred}(\hat{\Gamma})$  and  $\mathcal{N}_{pred}(\hat{\Gamma}, \mathcal{D}_{test})$  when restricting the range for one of the inputs  $\alpha_0, \nu, \rho, K$ , and  $T$  into  $[Q_k, Q_{k+1}]$ . Here,  $[Q_k, Q_{k+1}]$  is a subset containing the bottom 20% to 20(k + 1)% of a given set.

ordinary least squares (OLS) is employed in this study. The MC produces larger standard deviations  $\beta_l$  on the specific domains. Although the targets  $\sigma_{approx,l}^I$  for regression have different  $\beta_l$ , if OLS is adopted, the capacity of the network can be exhausted due to  $\sigma_{approx,l}^I$  with large deviations. Thus, the weighted least squares (WLS) should be used to resolve it. However, estimating the deviations  $\beta_l$  to utilize the WLS may be considerably difficult.

Finally, we reflect on the distribution of a random sample  $\epsilon_{pred}$  from  $\mathcal{D}_{pop}$ , where  $\mathcal{D}_{pop}$  is the population producing  $\epsilon_{pred,l}(= \sigma_{net,l}^I - \sigma_{true,l}^I)$ . (Roughly,  $\mathcal{D}_{pop} = \{\epsilon_{pred,l}\}_{l=1,\dots,\infty}$  in that the population can be understood as the set of infinite samples.) By doing so, we can guess how well  $\{\sigma_{net,l}^I\}_{l=1,\dots,L'}$  approximates  $\{\sigma_{true,l}^I\}_{l=1,\dots,L'}$ . For instance, we can talk about  $P[|\sigma_{net,l}^I - \sigma_{true,l}^I| < 1\text{bp}]$ . First,  $E[\epsilon_{pred}] = 0$  because  $E[\sigma_{pred,l}^I] = 0$  (see relation (2)). Moreover, because  $Var[\epsilon_{pred}] = E[\mathcal{E}_{pred}(\hat{\Gamma})]$ ,  $Var[\epsilon_{pred}]$  is estimated as 2.03E-07 as depicted in Table 5. This association signifies that if the best performance network (i.e., 4 layers and 7,000 nodes per hidden layer) is utilized,  $std[\epsilon_{pred}]$  is about 0.00045 (0.45bp). Thus, under the assumption that  $\epsilon_{pred}$  follows a normal distribution, approximately 97% of  $|\epsilon_{pred}|$  are within 1bp. This outcome obviously has remarkable accuracy. However, the normal assumption for the claim is hard to prove because estimating higher moments of  $\epsilon_{pred}$  is difficult at the moment. Alternatively, we try to draw many plots of  $\sigma_{net}^I$  with respect to  $\log(K/f_0)$ , along with the 99% confidence intervals computed using 10 million MC simulations. We then confirm that most of  $\sigma_{net}^I$  are in the intervals. Owing to the limitation of space, we select two and draw them in Figure 5. In the figure, the blue regions indicate the 99% confidence intervals. The intervals are too thin to be observed, so auxiliary figures are drawn at the bottom, in which the intervals are drawn centered about  $\sigma_{net}^I$ . Notably, we can estimate the accuracy of the network through the subfigures. Based on the examination of the many plots, we speculate that the guess  $|\epsilon_{pred}| < 1\text{bp}$  with a high probability is not far wrong.

## 5. Conclusion

Recently, the application of deep learning algorithms has facilitated outstanding achievement in various fields. Considering that pricing options are truly essential in financial engineering, it seems inevitable to note recent research using artificial neural networks to predict the prices for particular parametric models. In our opinion, the models without any pricing formulas should be studied more intensively. Nevertheless, measuring prediction errors is virtually impossible because true prices are unknown for such types of models. To resolve this problem, we develop a novel method based on the Monte-Carlo simulation and nonlinear regression. According to the method, the best performance network developed in this work produces the results as accurate as those of 13 million MC simulations. It is a remarkable result because the MC takes much more computational time in comparison to the network.



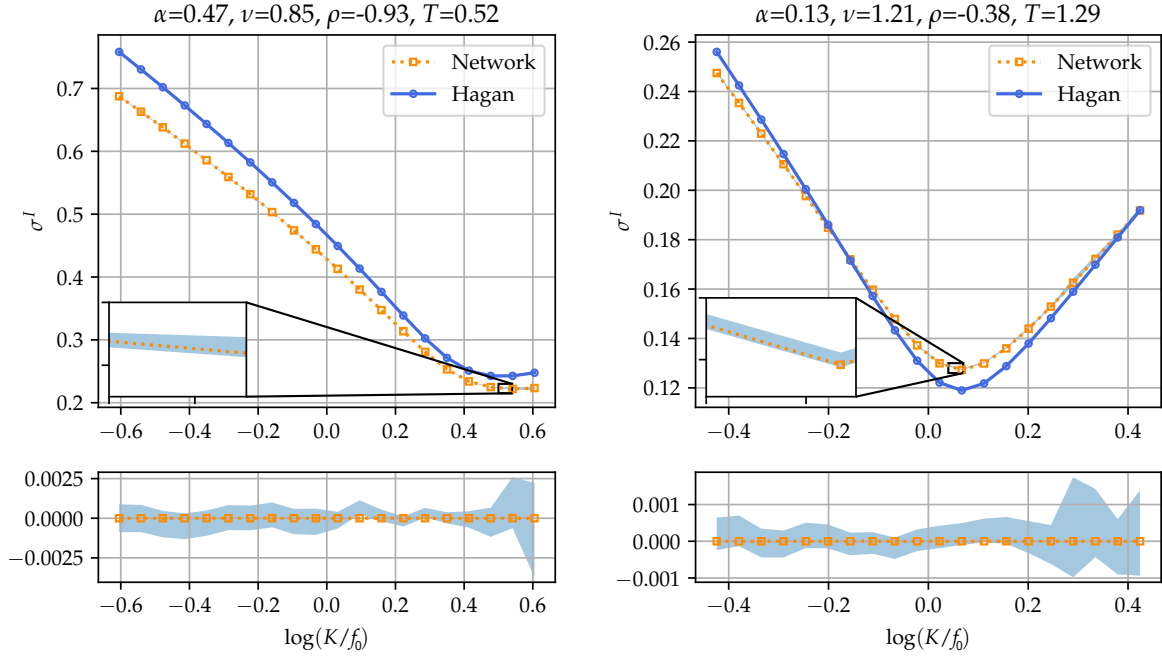


Figure 5: The figures highlight the predictions of the best performance network for the data in the test set  $\mathcal{D}_{test}$ . The blue regions indicate the 99% confidence intervals computed by 10 million MC simulations. The intervals are drawn again centered about  $\sigma_{net}^I$  in the auxiliary subfigures at the bottom.

There are unresolved problems for future research. First, the decreasing rate of the prediction errors does not exactly match with the value our theory predicts. This discrepancy implies that the theory should be improved to address the gap. Second, the weighted least square should be introduced because the simulated option prices have different variances. Finally, only the expectation and variance of the prediction errors are provided in this work, but it is more desirable to investigate the theoretical distribution of the errors.

## Acknowledgments

We are grateful to Korean Asset Pricing, a bond rating agency located in Korea, for providing data in Figure 1. Jaegi Jeon received financial support from the National Research Foundation of Korea (NRF) of the Korean government (Grant No. NRF-2019R1I1A1A01062911). Jeonggyu Huh received financial support from the NRF (Grant No. NRF-2019R1F1A1058352).

## References

- [1] G. Cybenko, Approximation by superpositions of a sigmoidal function, *Mathematics of control, signals and systems* 2 (1989) 303–314.
- [2] K. Hornik, M. Stinchcombe, H. White, et al., Multilayer feedforward networks are universal approximators., *Neural networks* 2 (1989) 359–366.
- [3] J. Ruf, W. Wang, Neural networks for option pricing and hedging: a literature review, Available at SSRN 3486363 (2019).
- [4] B. M. Henrique, V. A. Sobreiro, H. Kimura, Literature review: Machine learning techniques applied to financial market prediction, *Expert Systems with Applications* 124 (2019) 226–251.
- [5] J. M. Hutchinson, A. W. Lo, T. Poggio, A nonparametric approach to pricing and hedging derivative securities via learning networks, *The Journal of Finance* 49 (1994) 851–889.
- [6] F. Black, M. Scholes, The pricing of options and corporate liabilities, *Journal of political economy* 81 (1973) 637–654.

- [7] S. L. Heston, A closed-form solution for options with stochastic volatility with applications to bond and currency options, *The review of financial studies* 6 (1993) 327–343.
- [8] P. S. Hagan, D. Kumar, A. S. Lesniewski, D. E. Woodward, Managing smile risk, *The Best of Wilmott* 1 (2002) 249–296.
- [9] R. Culkin, S. R. Das, Machine learning in finance: the case of deep learning for option pricing, *Journal of Investment Management* 15 (2017) 92–100.
- [10] A. Broström, R. Kristiansson, Exotic derivatives and deep learning, 2018.
- [11] R. Ferguson, A. Green, Deeply learning derivatives, *arXiv preprint arXiv:1809.02233* (2018).
- [12] W. A. McGhee, An artificial neural network representation of the sabr stochastic volatility model, Available at SSRN 3288882 (2018).
- [13] S. Liu, C. W. Oosterlee, S. M. Bohte, Pricing options and computing implied volatilities using neural networks, *Risks* 7 (2019) 16.
- [14] A. Hirta, T. Karatas, A. Oskoui, Supervised deep neural networks (dnns) for pricing/calibration of vanilla/exotic options under various different processes, *arXiv preprint arXiv:1902.05810* (2019).
- [15] F. D. Rouah, *The Heston Model and Its Extensions in Matlab and C*, John Wiley & Sons, 2013.
- [16] J. Gatheral, T. Jaisson, M. Rosenbaum, Volatility is rough, *Quantitative Finance* 18 (2018) 933–949.
- [17] P. Wilmott, *Paul Wilmott on quantitative finance*, John Wiley & Sons, 2013.
- [18] P. Glasserman, *Monte Carlo methods in financial engineering*, volume 53, Springer Science & Business Media, 2013.
- [19] D. C. Montgomery, E. A. Peck, G. G. Vining, *Introduction to linear regression analysis*, volume 821, John Wiley & Sons, 2012.
- [20] P. C. Hansen, V. Pereyra, G. Scherer, *Least squares data fitting with applications*, JHU Press, 2013.
- [21] R. Rebonato, K. McKay, R. White, *The SABR/LIBOR Market Model: Pricing, calibration and hedging for complex interest-rate derivatives*, John Wiley & Sons, 2011.
- [22] G. West, Calibration of the sabr model in illiquid markets, *Applied Mathematical Finance* 12 (2005) 371–385.
- [23] B. Bartlett, Hedging under sabr model, *Wilmott magazine* 4 (2006) 2–4.
- [24] S. E. Shreve, *Stochastic calculus for finance II: Continuous-time models*, volume 11, Springer Science & Business Media, 2004.
- [25] J. Obloj, Fine-tune your smile: Correction to hagan et al, *Wilmott Magazine* 2008 (2008).
- [26] P. Henry-Labordere, *Analysis, geometry, and modeling in finance: Advanced methods in option pricing*, Chapman and Hall/CRC, 2008.
- [27] L. Paulot, Asymptotic implied volatility at the second order with application to the sabr model, *Large Deviations and Asymptotic Methods in Finance*, Springer (2015) (2009) 37–69.
- [28] Q. Wu, Series expansion of the sabr joint density, *Mathematical Finance: An International Journal of Mathematics, Statistics and Financial Economics* 22 (2012) 310–345.
- [29] A. Antonov, M. Konikov, M. Spector, Sabr spreads its wings, *Risk* 26 (2013) 58.
- [30] R. Garcia, R. Gençay, Pricing and hedging derivative securities with neural networks and a homogeneity hint, *Journal of Econometrics* 94 (2000) 93–115.
- [31] G. Dimitroff, D. Roeder, C. P. Fries, Volatility model calibration with convolutional neural networks, Available at SSRN 3252432 (2018).
- [32] C. Bayer, B. Horvath, A. Muguruza, B. Stemper, M. Tomas, On deep calibration of (rough) stochastic volatility models, *arXiv preprint arXiv:1908.08806* (2019).
- [33] D. P. Kingma, J. Ba, Adam: A method for stochastic optimization, *arXiv preprint arXiv:1412.6980* (2014).